Rotationally resolved (1+1 ') resonance-enhanced multiphoton ionization (REMPI) of CaR (R = H, D) in supersonic beams: CaR X (2)Sigma(+) (v ''=0) -> CaR* B (2)Sigma(+) (v '=0, 1) -...

ARTICLE *in* THE JOURNAL OF PHYSICAL CHEMISTRY A · NOVEMBER 2003

Impact Factor: 2.69 · DOI: 10.1021/jp036351s

Rotationally Resolved (1 + 1′) Resonance-Enhanced Multiphoton Ionization (REMPI) of CaR (R = H, D) in Supersonic Beams: CaR $X\ ^2\Sigma^+$ ($v'' = 0$) → $CaR^*\ B\ ^2\Sigma^+$ ($v' = 0, 1$) → $CaR^+\ X\ ^1\Sigma^+$

Khaled Gasmi,[†] Reem M. Al-Tuwirqi,[‡] Stefan Skowronek,[†] Helmut H. Telle,*[,†,§] and Angel González Ureña*[,†]

Instituto Pluridisciplinar, Universidad Complutense, Paseo Juan XXIII, 1 E - 28040 Madrid, Spain, Department of Physics, King Abdul Aziz University, P.O. Box 12559, Jeddah 21483, Saudi Arabia, and Department of Physics, University of Wales Swansea, Singleton Park, Swansea SA2 8PP, United Kingdom

Received: August 8, 2003; In Final Form: September 26, 2003

We report on a laser-spectroscopic study of the CaH and CaD radicals in a supersonic beam, generated in a reaction of laser-sputtered Ca atoms and a pulsed beam of H_2 or D_2, seeded in helium. The rotational levels of the electronic ground-state $X\ ^2\Sigma^+$ ($v'' = 0$, $N'' \leq 10$) were probed by two-color resonance ionization mass spectrometry—(1 + 1′) resonance-enhanced multiphonon ionization (REMPI)—via the intermediate $B\ ^2\Sigma^+$ ($v' = 0, 1$) rovibronic levels. Rotational constants for the *B*-state were derived, including the spin splitting parameters γ_v', which have been determined in the case of CaD for the first time: $\gamma_0 = -0.409(7)$ cm^{-1} and $\gamma_1 = -0.398(8)$ cm^{-1} for CaD ($B\ ^2\Sigma^+$), and $\gamma_0 = -0.792(15)$ cm^{-1} and $\gamma_1 = -0.765(16)$ cm^{-1} for CaH ($B\ ^2\Sigma^+$). The comparison between the rotational level energies of the F_1 and F_2 spin substates of the two isotopomers revealed the onset of perturbation in CaH $B\ ^2\Sigma^+$ ($v' = 0$), at $N' \cong 0$, by the presence of the vibronic state $A\ ^2\Pi$ ($v' = 1$). Although this perturbation is documented for $v' \geq 1$, it had not been previously recognized for $v' = 0$. The rotational populations observed in $X\ ^2\Sigma^+$ ($v'' = 0$) for the two isotopomers could be associated with different average rotational temperature values for CaD and CaH: $T_{rot} = 52\ (\pm 7)$ and $T_{rot} = 85\ (\pm 11)$ K, respectively.

1. Introduction

The monohydrides of alkali or alkaline-earth metal atoms, MH, or their isotopomers, MD, are frequently being considered as "textbook examples" for diatomic molecules, which allow molecular science to explore a variety of interesting, fundamental properties that involve molecular structure and dynamics. For example, many of these molecules exhibit rotational perturbations and electronic state interaction, and distinct state-dependent threshold behavior in their formation dynamics in the gas-phase reactions M/M* + H_2/D_2 is observed (the reaction paths that involve the metal atom M in its ground state are primarily endothermic).

Because of their relative simplicity, the metal (mono) hydrides have also attracted much interest from theoreticians, who tried to provide ab initio potential energy curves, reaction hypersurfaces, and transition-moment functions with sufficient accuracy to explain and model some of the observed irregularities in the spectra from a quantum chemical point of view. One further, practical reason for the interest in the spectroscopy of the metal hydrides lies in their astrophysical importance, and, in particular, CaH has attracted much attention (see, for example, the work of Barbuy et al.[1] and Balfour and Klynning[2]).

Traditionally, MH (or MD) molecules have been studied in hot gas cell arrangements, at pressures of a few millibars. The level populations are generally fully thermalized, at temperatures of typically a few hundred to a thousand degrees Kelvin. Although this means that a large number of rotational levels can be probed, and thus spectroscopic and dynamic parameters may easily be extracted to high precision, the high temperature means that the levels with the lowest rotational quantum number have only a small population. However, it is at the low rotational energy levels that perturbation is encountered in many of the excited potential energy states of metal hydrides.

In the study reported here, we followed a different experimental approach, in which the metal monohydride is provided within a supersonic molecular beam environment. Thus, the rotational temperature was only a few tens of degrees Kelvin, and, accordingly, only the lowest rotational energy levels carry a significant population. The ions of the MH/MD species under study were analyzed, after resonance-enhanced multiphonon ionization (REMPI) excitation, using time-of-flight mass spectrometry (ToF−MS). This constitutes a very sensitive detection mechanism, and furthermore, it allows mass and, hence, isotope selectivity as well. We demonstrated this approach for the hydrides of the alkaline-earth metal atom Ca. The Ca atoms were generated by laser ablation from a solid target and reacted with a pulsed H_2/D_2 beam; sufficient energy is provided in the laser ablation plasma to overcome the endothermic reaction barrier.

The method of radical preparation that is based on a chemical reaction between laser-ablated atoms and a reactive gas (seeded) molecular beam arrangement has been exploited since the late 1980s, initially in laser-induced fluorescence studies of metal-containing diatomic molecules, to name but a few representative examples: ZrS from the reaction Zr + OCS,[3] YF from the reaction Y + SF_6,[4] or ReN from the reaction Re + NH_3.[5] Probing of the product molecule by (1 + 1′) REMPI ToF−MS was introduced ~10 years later, e.g., BaF from the reaction of barium and FCH_3 via the intermediate complex $BaLFCH_3$,[6] or FeC from the reaction of iron and CH_4.[7] The latter is the first in a long series of metal atom−methane molecule catalysis studies by Morse and co-workers at the University of Utah, which now includes the metal carbides of cobalt, chromium,

* Authors to whom correspondence should be addressed. E-mail: h.h.telle@swansea.ac.uk, laseres@pluri.ucm.es.
[†] Instituto Pluridisciplinar.
[‡] King Abdul Aziz University.
[§] University of Wales Swansea.

10.1021/jp036351s CCC: $25.00
Published on Web 11/12/2003

iron, molybdenum, nickel, palladium, ruthenium, titanium, vanadium, and tungsten. Although all the aforementioned product molecules could also be liberated by ablating pressed pellets or alloy disks, as was demonstrated by us and other groups, the efficiency of generation in a gas flow reaction is normally superior,[7] because, in laser material ablation, molecular bonds are usually broken rather than maintained or formed. However, the generation of the product in a gas flow is indispensable if minor isotopes of the reagent are of interest, such as ^{2}H or ^{13}C with a natural abundance of 0.0156% and 1.108%, respectively. Isotopically "pure" reagent gases, such as D_2 and $^{13}CH_4$, must be used, as was demonstrated in laser-induced fluorescence measurements of, for example, CoH/CoD from the reaction of cobalt with H_2/D_2,[8] or $Y^{12}C/Y^{13}C$ from the reaction $Y + {}^{12}CH_4/{}^{13}CH_4$.[9]

To our knowledge, no isotope-specific experiments that exploit REMPI ToF−MS, other than our CaH/CaD from the reaction of calcium with H_2/D_2, have been reported to date.

The diatomic reaction products CaH and CaD were expanded to form a supersonic beam and were probed, exploiting the (1 + 1′) REMPI excitation path CaR ($X\ ^2\Sigma^+$) → CaR ($B\ ^2\Sigma^+$, $A\ ^2\Pi$) → CaR^+ ($X\ ^1\Sigma^+$). Some early experimental results for CaH that are related to this study, and their preliminary analysis, have been reported recently.[10]

One major reason for the particular choice of transitions was that the lowest electronic states of CaH, namely, $B\ ^2\Sigma^+$ and $A\ ^2\Pi$, are similar in potential energy, and their anharmonicity constants are almost equal. In the low-v' CaH $A(v' + 1)/B(v')$ vibrational pairs, typical energy-level perturbation is observed for the rotational spin sublevels F_2, as a consequence of the close proximity of some low-lying rotational levels of equal parity.[11,12]

The perturbation is encountered only for CaH but is completely lifted for CaD, at least in the range of rotational levels that are accessible in supersonic beam experiments at low rotational temperatures. This is due to the huge isotope shift in the vibrational energy term pairs $A(v' + 1)/B(v')$ in CaH and CaD; thus, low rotational quantum levels remain unperturbed (for further details, see Section 3.2). This different behavior could be exploited, in principle, to extract unperturbed spectroscopic constants from the CaD data and generate the equivalent unperturbed constants for CaH, without the need for complex deperturbation procedures, such as those used by Berg and co-workers,[11] by exploiting the well-known and usually rather precise isotopic mass dependence of the spectroscopic parameters.[13,14]

Although both the $B\ ^2\Sigma^+$ and $A\ ^2\Pi$ electronic states of CaH and CaD could be probed in our experiments, here, we have restricted our presentation to the results from the $X\ ^2\Sigma^+ \rightarrow B\ ^2\Sigma^+$ transition, namely, the two vibrational bands ($v'' = 0 \rightarrow v' = 0, 1$). For these bands, the principle of isotopomer correlation of the spectroscopic data is exemplified. The rovibrational bands of the $X\ ^2\Sigma^+ \rightarrow A\ ^2\Pi$ transition will be the subject of a forthcoming publication.

2. Experimental Section

As noted in the Introduction, in almost all published investigations of (gaseous) CaH/CaD, the molecule was formed by heating metallic calcium to ~1000−1200 K in an atmosphere of hydrogen (or deuterium), at pressures of typically a few millibars. The resultant "hot" vibrational−rotational bands of the $A-X$ and $B-X$ electronic transitions of CaH were probed by classical emission/absorption spectroscopy[15,16] and laser fluorescence spectroscopy.[11,12] To our knowledge, no information for these transitions has been published for CaD; only fragmentary information was available to us.[17] For simplicity, we will mostly use the expression CaR, with (R = H, D), when discussing features and properties that are related to both isotopomers CaH and CaD.

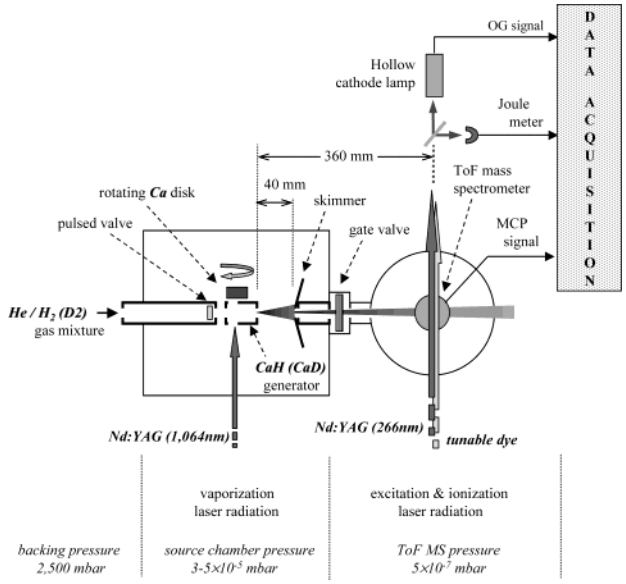

Figure 1. Schematic diagram of the experimental resonance ionization mass spectrometry (RIMS) setup for CaH/CaD. Resonant absorption and ionization through tunable- and fixed-frequency laser radiation. Ion detection through time-of-flight (ToF) mass analysis (ToF tube perpendicular to the plane of the molecular and laser beams).

In the present study, CaR was formed in a reaction of laser-sputtered calcium with H_2/D_2 gas in injected through a pulsed valve; subsequently, CaR was expanded into a supersonic molecular beam, resulting in "cold" vibrational and rotational level population distributions. Probing of the ground-state level distribution was made by resonant excitation into an (electronic) excited intermediate state and subsequent photo-ionization out of this intermediate state, using a second excitation photon, and then detecting the CaR^+ ion using ToF−MS equipment with a multichannel plate detector. The ion signal pulses were amplified and recorded using a digital storage oscilloscope (DSO; TDS-540, Tektronix), which allowed for a running average over a series of laser pulses. A personal computer was used for the accumulation and evaluation of the data provided by the DSO. The principle of this mass-selective (1 + 1′) REMPI setup is shown in Figure 1; for further details of the apparatus, see, for example, Skowronek et al.[6]

The schematic partial vibrational energy level structure for the $X\ ^2\Sigma^+$, $B\ ^2\Sigma^+$, and $A\ ^2\Pi$ states of CaH and CaD is shown in Figure 2, together with the two-step two-color resonance ionization excitation schemes used in this study. The relevant REMPI transition wavelengths for probing the individual rotational/vibrational levels of CaR ($X\ ^2\Sigma^+$) via the intermediate electronic states CaR ($A\ ^2\Pi$, $B\ ^2\Sigma^+$) are indicated.

For the recording of the CaR spectra, out of the complete ToF mass spectra only the time slice corresponding to m_{CaH} = 41 amu or m_{CaD} = 42 amu was sampled. This sampling restriction was required, because large amounts of Ca^+ ions are generated by multiphoton ionization; without mass selection, these would mask the small CaR ion signal. An example for the relevant mass spectrum section, in the range of 39.5−44.5 amu, is shown in Figure 3. The $^{40}Ca^1H/^{40}Ca^2H$ mass signal contributions, for the excitation laser tuned to the ($X-B$,0−0) $P_1(1)$ transition line, is of the same order of magnitude as are the peaks of the minor ^{42}Ca and ^{44}Ca isotopes. Note that the resolution of the ToF−MS system over the mass range of interest is $m/\Delta m \cong 1000$; thus, all relevant mass peaks are well-

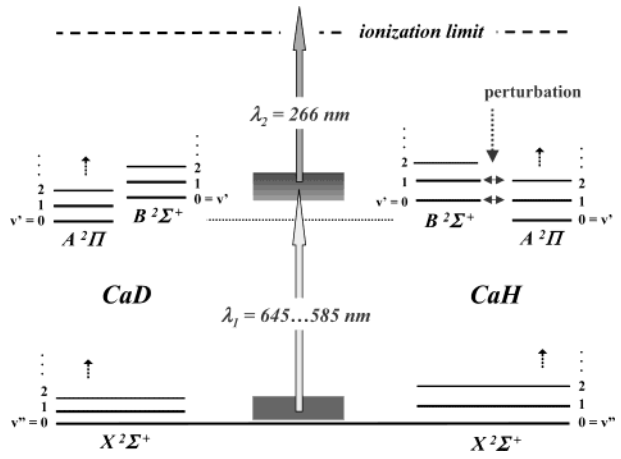

Figure 2. Schematic vibrational term level diagram of the $X\ ^2\Sigma^+$, $B\ ^2\Sigma^+$, and $A\ ^2\Pi$ states of CaH and CaD, and the two-step two-color resonance ionization scheme. Energy axis not to scale.

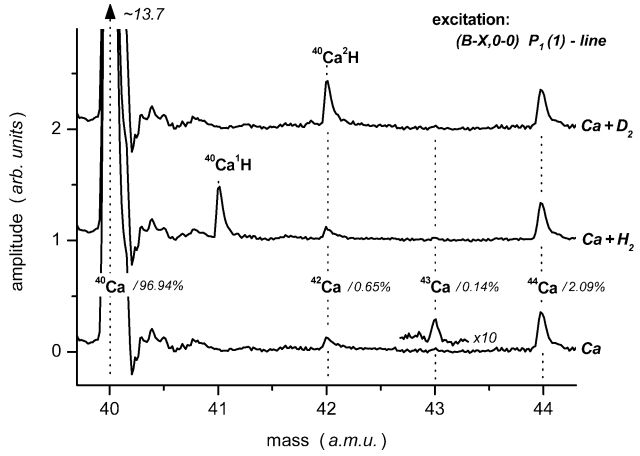

Figure 3. Typical ToF mass spectra in the mass range of $m = 39.5-44.5$ amu (including ^{40}Ca, $^{40}Ca^1H$, $^{40}Ca^2H$, ^{42}Ca, ^{43}Ca, and ^{44}Ca), recorded for the ($X-B$, 0−0) $P_1(1)$ transition line. Bottom trace represents CaR with the excitation off; middle trace represents CaH with the excitation on; and top trace represents CaD with the excitation on. For the sake of clarity, traces are offset from each other. For details, see text.

separated but the subtle mass differences between the atomic and molecular peaks of the same principal mass number are not resolved.

The figure may also serve as an indication of the compromise one must make to optimize the ionization step for CaR detection. High fluences of the ionization laser radiation would normally be desirable to increase the fraction of ionization; however, nonresonant ionization of Ca would increase dramatically as well. Thus, the $^{40}Ca^1H$ signal would sit on the tail of the large ^{40}Ca peak (the tail is comprised predominantly of the electronic RC detector time constant and AC amplifier oscillations). This can introduce large background fluctuations, which might easily mask weak CaH rotational lines.

The problem of (nonresonant) background contributions from Ca atoms is even more problematic when acquiring the $^{40}Ca^2H$ (CaD) mass signal. This signal is superimposed on the ever-present contribution from ^{42}Ca; any increase, or fluctuation of the latter's magnitude would severely diminish the signal-to-noise ratio for the molecular component. As a result, the recording of CaD spectra was rather more tedious than that for CaH, as manifested by the fluctuating baseline and stronger variations in the relative rotational line intensities (for further details, see Section 3.2).

Note that, in the experiments with Ca + H_2, the mass peak at $m = 42$ amu is not only due to the ^{42}Ca isotope but also comprises a small contribution from the triatomic molecule $^{40}Ca(^1H)_2$. This was confirmed in reference test measurements, in which no H_2 was added to the helium carrier gas, and thus only signals from a pure Ca atom were observed.

Of equal importance to the fluences of the *ionization* laser was the choice of energy density within the *excitation* laser beam, which induces the transitions $X \rightarrow A, B$. Even with the moderate maximum pulse energies of ~1 mJ available from the dye laser saturation and power broadening were observed, and care needed to be taken in selecting suitable laser light fluences. Experiments were performed at laser energy densities of ~1.25 mJ/cm^2, which guaranteed reasonably strong line intensities at sufficient spectral resolution, while maintaining (mostly) a Lorentzian line profile.

3. Results

The overall purpose of the research reported in this study was to investigate the ground and first electronically excited $^2\Sigma^+$ states of CaR, i.e., the *X*- and *B*-states, applying isotope-selective (1 + 1′) REMPI.

Because of the two-step resonant ionization that is required to generate the CaR^+ ions for mass spectrometric detection, some understanding of the molecular spectroscopy related to the excitation of the two close-lying intermediate electronic states CaR*($A\ ^2\Pi$) and CaR*($B\ ^2\Sigma^+$) is required. A very brief summary of the features expected in the recorded spectra is given below, before individual spectral data are discussed.

3.1. Spectroscopy of the Transition CaR ($X\ ^2\Sigma^+ - B\ ^2\Sigma^+$). The transition-line structure of CaR can be described by Hund's case (*b*), at least for the low rotational quantum levels observed in this study. Hence, one expects to observe six line branches, namely P_1, P_2, $^PQ_{12}$, $^RQ_{21}$, R_1, and R_2. As is customary, the indices "1,2" refer to the two spin substates F_1 and F_2 with $J = N + {}^1/_2$ and $J = N - {}^1/_2$.

Because of the very small spin splitting constant of the ground vibrational state ($X\ ^2\Sigma^+$, $v'' = 0$) of γ_0(CaH) = 0.04670 cm^{-1} and γ_0(CaD) = 0.02174 cm^{-1} (see Petitprez et al.[18]), some of the braches cannot be resolved from each other, because of the line width of the probe laser being of the same order as the spin splitting. Thus, the nominal six branches are reduced to four apparent branches, and P_1/Q_{12} and R_2/Q_{21} remain unresolved. The "broadening" of the line profiles related to the latter branches, which is observed with increasing rotational quantum number, is indicative of the ground-state spin splitting just starting to become observable.

On the basis of the gas pressures and the expansion geometry encountered in our CaR supersonic beam, a rotational temperature of the order 30−40 K would be expected, meaning that rotational levels up to $N'' \cong 10$ should be sufficiently populated to be observed with a reasonable signal-to-noise ratio in the resonance ionization mass spectrometry (RIMS) spectra.

For molecules with large vibrational energy-level spacing, such as CaR, one normally finds that the lowest vibrational level $v'' = 0$ carries the bulk of the population, even for vibrational temperatures remaining as high as a few hundred Kelvin. For example, in CaH the vibrational levels v''=1 and v''=2 would carry a fractional population of only 2.3×10^{-3} and 6.6×10^{-6} at $T_{vib} = 300$ K, relative to $v'' = 0$. Only occasionally did we observe hints at the presence of $v'' = 1$; contributions from any higher vibrational level remained below the noise level. Hence, we conclude that the vibrational temperature in our supersonic beam RIMS experiments was of the order of $T_{vib} =$ 300−400 K at the most. Note that, in cell experiments with

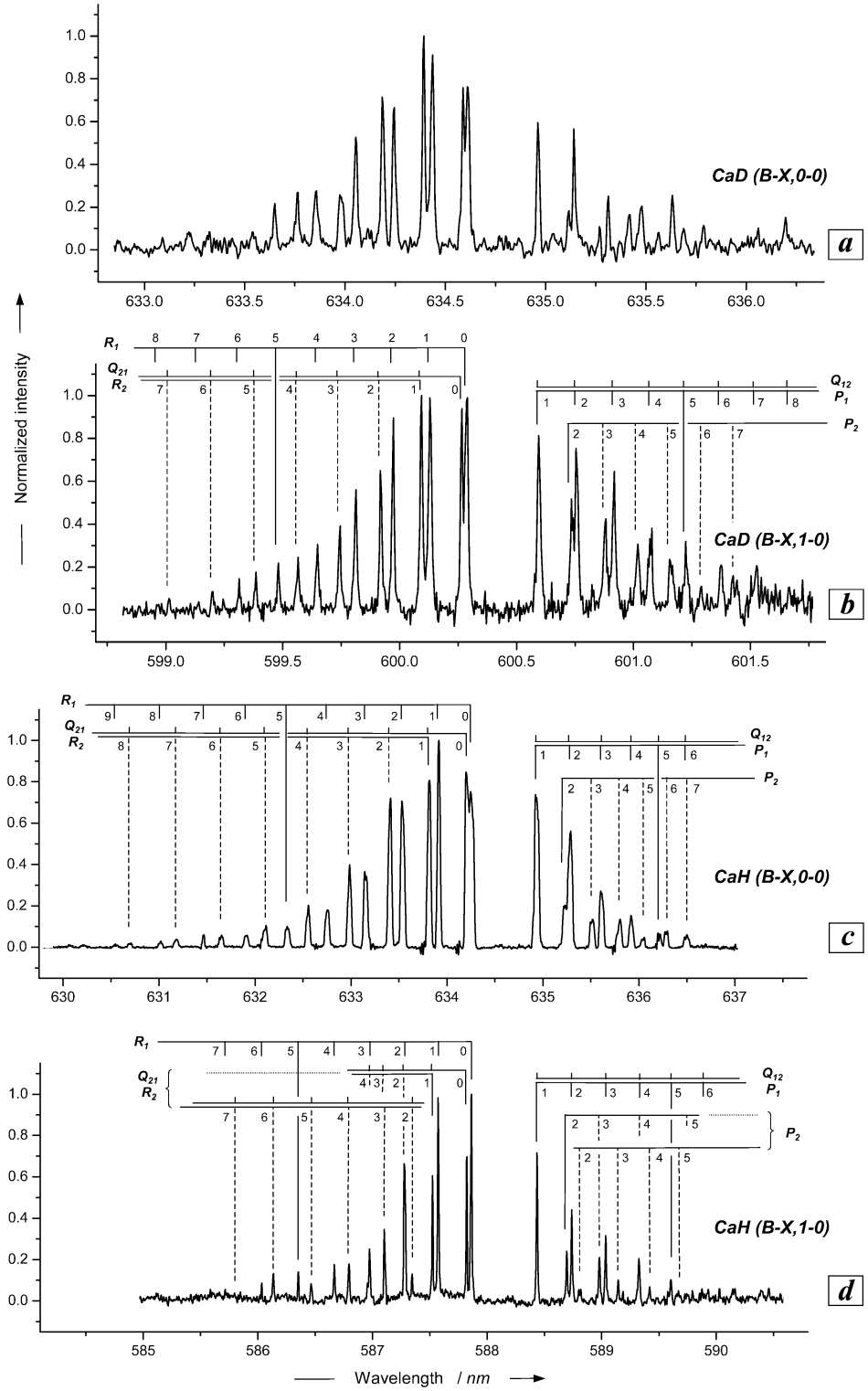

Figure 4. (1 + 1′) REMPI spectra of CaD/CaH ($X,v'' \rightarrow B,v'$): (a) CaD (0−0) band; (b) CaD (0−1) band; (c) CaH (0−0) band, extracted from the mixed spectrum ($X,v'' = 0 \rightarrow B,v' = 0/A,v' = 1$); (d) CaH (0−1) band. Selected rotational branches are indicated. The intensities are normalized to the strongest rotational line, and wavelength scale is normalized to the P-/R-branch origin gap. See text for further details.

typical temperatures of $T_{rot} \cong T_{vib} = 1000-1100$ K, the fractional population in $v'' = 1$ and $v'' = 2$ would be 0.164 and 0.028, respectively.[11,17]

When considering the Franck−Condon factors (FCF) and the dipole transition moments (A-values)—calculated using the computer code by Telle et al.[19] and data from Leininger and Jeung[20]—for the vibrational bands of the CaR ($X-B$) system, in addition to the supersonic beam temperature arguments, the number of observable bands is further constrained in our experiments. In fact, only two vibrational bands are needed to be considered in the analysis, namely ($v'' = 0 \rightarrow v' = 0$) with $FCF_{XB,00} = 9.8510 \times 10^{-1}$ and ($v'' = 0 \rightarrow v' = 1$) with $FCF_{XB,01} = 1.3692 \times 10^{-2}$. All other bands were disfavored by very low vibrational population and/or very small FCF values.

3.2. CaR (*X*, *v*″ = 0 − *B*, *v*′ = 0, 1) Band Spectra. Representative spectra for CaR(X, $v'' = 0 - B$, $v' = 0, 1$) are shown in Figure 4; for ease of comparison, all traces were normalized to the intensity of the strongest observed rotational

TABLE 1: Rotational Energy Levels for the CaD and CaH Transitions Investigated in This Study[a]

	CaD ($B\,^2\Sigma^+$, $v'=0$) (cm^{-1})		CaD ($B\,^2\Sigma^+$, $v'=1$) (cm^{-1})		CaH ($B\,^2\Sigma^+$, $v'=0$) (cm^{-1})		CaH ($B\,^2\Sigma^+$, $v'=1$)[b] (cm^{-1})		
N'	T_1	T_2	T_1	T_2	T_1	T_2	T_1	T_2 (i)	T_2 (ii)
0	16211.529		17112.430		16398.087		17642.292		
1	16215.790	16216.408	17116.659	17117.215	16406.491	16407.677	17650.526	17651.671	?
2	16224.561	16225.660	17125.310	17126.296	16423.697	16425.994	17667.354	17668.761	17673.920
3	16237.968	16239.331	17138.411	17139.832	16449.885	16452.798	17692.833	17692.636	17697.809
4	16255.849	16257.537	17155.956	17157.716	16484.771	16488.869	17727.022	17723.028	17732.099
5	16278.160	16280.422	17177.901	17180.138	16528.745	16533.410	17769.789	17761.114	17775.430
6	16305.058	16307.728	17204.239	17206.814	16581.203	16586.770	17820.909	?	17827.171
7	16336.482	xxx	17235.046	17238.115	16642.542	16648.746	17880.987		xxx
8	16372.534	16375.638	17270.348	17273.667	16712.635	16719.432	xxx		xxx
9	xxx	xxx	17309.881	xxx	16791.202	16798.845	xxx		xxx
10	xxx	xxx	xxx	xxx	16878.499	16886.725	xxx		xxx

[a] The values of the terms T_1, T_2 for the electronic excited-state $B\,^2\Sigma^+$ are derived from fits to the measured spectral line positions, utilizing the constants B_v, D_v, and γ_v that have been derived in this work; the values of the terms for the electronic ground state $X\,^2\Sigma^+$ are calculated from the rotational constants tabulated by Frum and Picket[21] and the vibrational constants tabulated by Petitprez et al.[18] [b] (i), (ii) denote perturbed rotational levels in the F_2 branch, with "extra" levels. [c] ? indicates that the rotation energy was not observed/identified, the intensity was at or below the noise level, or the line was fully masked by another stronger line. [d] xxx indicates that the line fit did not converge.

line, and the wavelength scale was stretched in such a way that, in the traces, the band origin gap between the R_1 and P_1 branches seems to be equal. We would like to make a few initial general remarks.

First, the spectra for CaD (Figure 4, traces a and b) exhibit a signal-to-noise ratio that is worse than that for CaH, despite all major experimental conditions being equal. This confirms the earlier statement (Section 2) that the mass interference $^{42}Ca/^{40}Ca^2H$ introduced a significant, fluctuating background into the molecular spectra.

Second, the spectrum for ($X-B$,0−0) band system of CaH (trace c in Figure 4) exhibits overlap with the CaH (X, $v''=0$ − A, $v'=1$) band, whose spectral has been subtracted, and only the CaH (X, $v''=0$ − B, $v'=0$) lines remain. The full mixed spectrum is shown in Figure S.1 in the Supporting Information section. The P lines with high rotational quantum numbers from the $X\,^2\Sigma^+$ ($v''=0$) − $B\,^2\Sigma^+$ ($v''=0$) transition are "missing", being completely masked by the dense line spectrum of the $X\,^2\Sigma^+$ ($v''=0$) − A $^2\Pi_{3/2}$ ($v'=1$) transition.

Third, all recorded band systems look relatively similar, for both isotopomers CaD and CaH, and for both sequences ($v''=0-v'=0$) and ($v''=0-v'=1$). This is not surprising, considering the similarities in the potential energy curves for the ground and excited states $X\,^2\Sigma^+$ and $B\,^2\Sigma^+$. Only at the higher rotational levels does the line spacing begin to diverge.

With only so few rotational levels available for analysis, for most branches of $N<10$, we did not attempt to extract the full set of general rotational spectroscopic constants (e.g., in the form of Dunham coefficients) for the excited electronic state CaR-($B\,^2\Sigma^+$), because there would be too many parameters to be fitted for the available data points. Instead, we tabulated the rotational energy levels, which we extracted from the transition lines ending at the same upper level, by subtracting the accurately known energies of the ground electronic state (calculated from tabulated constants[18,21]). All experimental energy-level values T_1 and T_2 (given in units of cm^{-1}) evaluated for $B\,^2\Sigma^+$ are collected in Table 1. Note that all values are referenced to the minimum of the $X\,^2\Sigma^+$ potential, i.e., for the absolute energy scale, the vibrational-energy term $G_{v''=0}$ was added to the lowest rotational energy level in the ground state, i.e., the ($X\,^2\Sigma^+$, $v''=0$, $N''=0$, $J''=1/2$) level (see the transition line and energy-level schematic in Figure 5 and the ground-state spectroscopic parameters in Table 2).

As mentioned previously, the close proximity of the vibrational levels $A(v'+1)/B(v')$ in CaH leads to rotational level perturbation (see energy-level schematics in Figure 2). This has

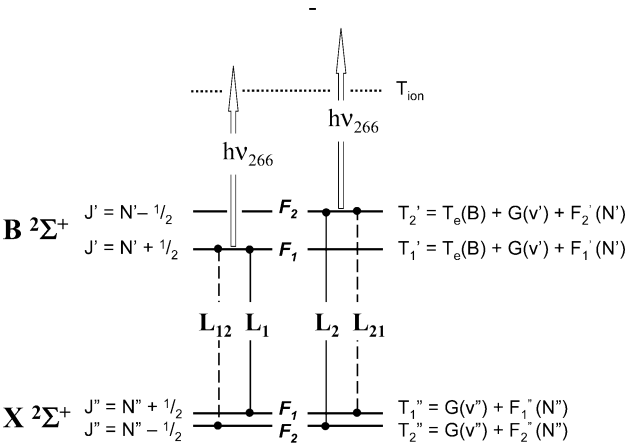

Figure 5. Principle of energy-level structure and transition lines for the determination of term values, spectroscopic constants, and level populations.

been reported for the vibrational levels $v'=1$, 2 in the $B\,^2\Sigma^+$ state, with the perturbation occurring in the vicinity of the rotational levels with quantum numbers $N_{(v'=1)} \cong 3$ and $N_{(v'=2)} \cong 6$, respectively.[11,12] In the ($X-B$,0−1) spectrum in Figure 5, the perturbation at $N_{(v'=1)} \cong 3$ is easily recognized: line positions are shifted significantly, in comparison with the evenly spaced pattern of the other transition spectra, and the line intensities deviate substantially from those expected, according to standard line strength (Hönl-London) factors $S_{J'J}$. Furthermore, one observes "additional" lines, giving the typical appearance of a double sequence that originates from a sharing of transition probability between perturbed and perturbing energy levels. The appearance of the theoretically expected energy spacing and intensity variation patterns is well-documented (see, for example, ref 22), and the patterns observed in the spectrum of CaH ($X-B$,0−1)—bottom trace in Figure 4—is in good agreement with theoretical expectations. Our spectral line positions also agree well with those derived from the CaH ($X-B$,1−1) band system tabulation in the work of Martin;[12] unfortunately, no line intensities are reported by Martin, so a full comparison was not possible.

Because of insufficient population in the vibrational levels $v''>0$ and the unfavorable FCF values for the transition bands with $\Delta v>1$, CaH $B\,^2\Sigma^+$ ($v'=2$, 3) could not be fully probed. Thus, an investigation of the perturbation in those vibrational levels was not possible.

No perturbation was reported for $v'=0$; however, as will be evident from our analysis below, the onset of perturbation

TABLE 2: Molecular Constants for the $X\ ^2\Sigma^+$ and $B\ ^2\Sigma^+$ States of CaH and CaD

symbol	CaH ($X\ ^2\Sigma^+$), from Frum and Pickett[21] (cm^{-1})	CaD ($X\ ^2\Sigma^+$), from Petriprez et al.[18] (cm^{-1})	CaH ($B\ ^2\Sigma^+$) (cm^{-1})		CaD ($B\ ^2\Sigma^+$), this work (cm^{-1})
			from Martin[12]	this work	
		vibration, G_v			
G_0[a]	644.409	462.509			
G_1[a]	1904.583	1372.824			
		rotation, B_v			
B_0	4.228689(22)	2.176956(13)	4.3455(3)	4.413(10) 4.385 calc[b]	2.256(6)
B_1	4.131728(23)	2.141386(15)	4.2244(4)	4.310(12) 4.274 calc[b]	2.215(5)
B_e[c]	4.277170	2.194741		4.464 4.441 calc[b]	2.277
α_e[c]	-9.696×10^{-2}	-3.557×10^{-2}		-0.103 -0.112 calc[b]	-0.041
		distortion, D_v			
D_0	$1.8498(13) \times 10^{-4}$	$4.8896(50) \times 10^{-5}$	$2.027(4) \times 10^{-4}$	$2.124(72) \times 10^{-4}$[d]	$5.32(55) \times 10^{-5}$[d]
D_1	$1.8483(14) \times 10^{-4}$	$4.8848(55) \times 10^{-5}$	$2.01(1) \times 10^{-4}$	$2.050(85) \times 10^{-4}$[d]	$5.28(48) \times 10^{-5}$[d]
		spin splitting, γ_v			
γ_0	$4.3569(87) \times 10^{-2}$	$2.174(24) \times 10^{-2}$		$-0.792(15)$ -0.796 calc[b]	$-0.409(7)$
γ_1	$4.2102(88) \times 10^{-2}$	$2.115(23) \times 10^{-2}$		 -0.765 calc[b]	$-0.398(8)$
γ_e[e]	4.4303×10^{-2}	2.2035×10^{-2}	-0.8	 -0.810 calc[b]	-0.415
α_γ[e]	-1.467×10^{-3}	-5.9×10^{-4}		 0.030 calc[b]	0.011

[a] Calculated from the Dunham coefficients in refs 18 and 21. [b] The term calc refers to CaH values calculated from CaD values, using isotope conversion factors. [c] Extracted from B_0 and B_1 (for details, see text). [d] From quadratic fit to the term values in Table 1 (for details, see text). [e] Extracted from γ_0 and γ_1 (for details, see text).

is noticeable, even for this vibrational level. Indeed, the full perturbation as seen for $v' = 1$, 2 would be expected at $N_{(v'=0)} \cong 0$ or 1. This would be consistent with the trend observed in the higher vibrational levels of CaH $B\ ^2\Sigma^+$: the lower the vibrational quantum number, the smaller the rotational quantum number (in increments of approximately three rotational quanta) at which perturbation occurs. However, the region of full perturbation is not encountered in (B,$v' = 0$), because the lowest rotational level in the perturbing electronic state $^2\Pi_{3/2}$ is $N' = 2$.

The problem of the aforementioned perturbation is almost completely lifted in the case of CaD (compare Figure 2). This is due to the huge isotope shift in the vibrational energy term, which, for the specific case of the vibrational pairs $A(v' + 1)/B(v')$ in CaR, amounts to $\sim$350 cm^{-1}. Consequently, rotational levels with equal quantum characteristics are no longer close enough to perturb each other. This is evident in the X, $v'' = 0 \rightarrow B$, $v' = 0$ band of CaD, which now stands completely isolated (compare the top traces in Figure 4). Thus, without any perturbation, extraction of the spectroscopic parameters for CaD should be possible, and using the well-known isotope relations for these parameters, the unperturbed values for CaH could be inferred. Examples for this are discussed in the following section.

3.3. Extracting Spectroscopic Parameters from the Spectra. For "simple" rotational spectra such as $^2\Sigma^+ - {}^2\Sigma^+$ transitions, it is normally straightforward to apply standard line-difference formulas to derive a range of rotational spectroscopic parameters, provided that the line sequences are "well-behaved" (for the principle of the line and level assignment used here; see Figure 5). Specifically, we investigated the spin splitting parameter γ_v for the two observed vibrational levels of the $B\ ^2\Sigma^+$ states. The evaluation of the energy differences in the P_1/P_2 and R_1/R_2 line pairs, for the same rotational quantum number N, yields a simple expression for the spin splitting constants γ_v for the particular vibrational level v that is involved in the transitions.[13]

Because the ground-state spin splitting contributions γ_0'' and γ_1'' in CaR ($X\ ^2\Sigma^+$) are known to very high accuracy,[21] their contribution can be subtracted from the line-difference data to yield an expression depending solely on γ_v' and N' for R and P lines with the same upper rotational quantum number N':

$$\Delta\nu_{12}(P(N' + 1)) - \gamma''(N' + 0.5) = \Delta\nu_{12}(R(N' - 1)) - \gamma''(N' - 1.5) = \gamma'(N' + 0.5) \quad (1)$$

Thus, by plotting the left-hand side of eq 1 for both the P- and R- branches, as a function of N', a linear dependence should be encountered, with a slope equal to the value of γ_v' and an intercept of $^1/_2\gamma_v'$. Any deviation from this linear behavior (for low rotational quantum levels) may serve as an indication for rotational level perturbation; this argument will be used in the discussion of results further below.

3.3.1. Spin Splitting in CaD ($B\ ^2\Sigma^+$, $v = 0$, 1). For the two vibrational levels $v' = 0$, 1, only for six and eight rotational levels, respectively, were transition pairs measurable with a sufficient signal-to-noise ratio to be included in the evaluation. The related energy differences are plotted in Figure 6 (in panels a and b); note that, for clarity, the P and R data points are offset from each other.

A linear fit of $f(N) = a + bN$ to the difference data should provide the spin splitting parameters γ_v' from the slope b; the intercept a for $N' = 0$ should be equal to $^1/_2\gamma_v'$, according to eq 1. The fit parameters for the two vibrational levels were $a = -0.214$ ($\pm$ 0.049) cm^{-1} and $b = -0.410$ ($\pm$ 0.007) cm^{-1} for the vibrational level $v' = 0$, and $a = -0.190$ ($\pm$ 0.035) cm^{-1} and $b = -0.399$ ($\pm$ 0.008) cm^{-1} for the vibrational level $v' = 1$. From the intercept value, which is $a = b/2$ within the least-squares fit error, with confidence limits of $R^2 > 0.96$, one also can infer that, indeed, the rotational energy levels are unperturbed, within the measurement accuracy.

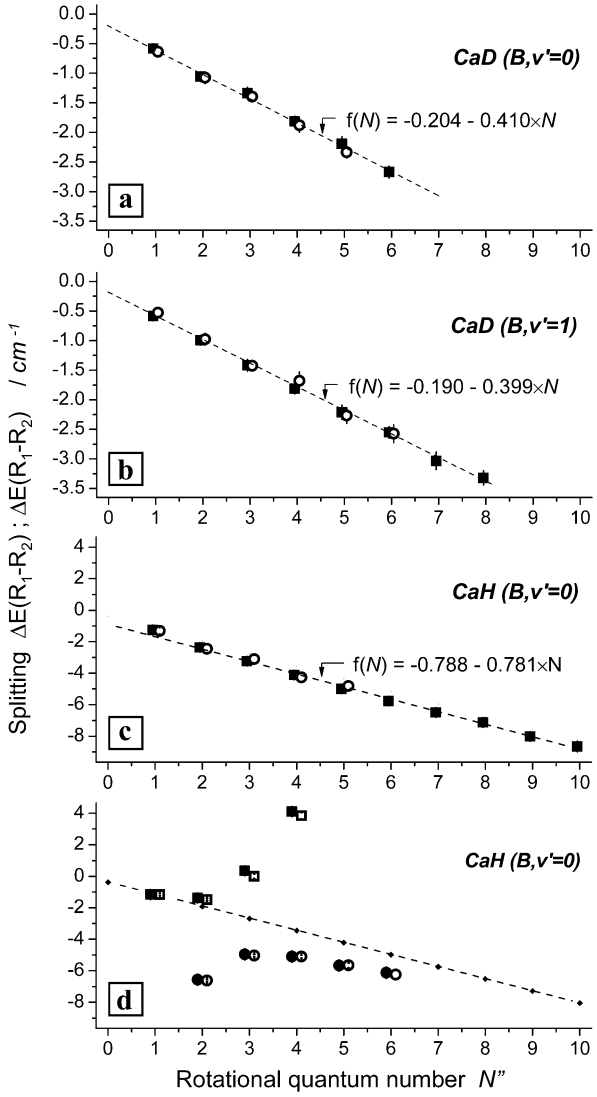

Figure 6. Spin splitting between F_1/F_2 rotational sublevels, derived from P_1/P_2 and R_1/R_2 line pair differences: (a) CaD ($B,v' = 0$), fit for $N' = 1, ..., 6$; (b) CaD ($B,v' = 0$), fit for $N' = 1, ..., 8$; (c) CaH ($B,v' = 0$), fit for $N' = 2, ..., 9$; and (d) CaH ($B,v' = 0$). Data are fits to the average of the line pairs. Solid symbols represent R-line data, and open symbols represent P-line data; the P and R data points are offset from each other for clarity. In panel d, the solid diamond data points along the dotted line represent data calculated from CaD ($B,v' = 1$).

From the two values for γ_0' and γ_1', one can derive a first estimate for the vibrational dependence of the spin splitting for CaD ($B\,^2\Sigma^+$), according to the expansion $\gamma_v' = \gamma_e' - \alpha_\gamma' \times (v + {}^1/_2) + ...$ Only two values have been measured; therefore, the (polynomial) approximation with the zero-order and first-order expansion coefficients must be treated with caution and any extrapolation to higher vibrational levels may be incorrect (specifically considering the irregular shape of the B/B' double minimum potential). The fitted values γ_0' and γ_1', and the derived parameters γ_e' and α_γ', are collected in Table 2. No values for the spin splitting in the excited CaD ($B\,^2\Sigma^+$) have been previously measured or reported.

3.3.2. Spin Splitting in CaH ($B\,^2\Sigma^+$, $v' = 0, 1$). Because of the much better signal-to-noise ratio in the CaH measurements, transition-line pairs were measurable for rotational levels up to $N' = 10$, albeit for $N' \geq 6$ P-lines were severely masked by other transition lines in the ($B-X$, 0−0) band system (see the spectrum in Figure 4); hence, those lines were not included in the evaluation procedure. The related energy differences are plotted in Figure 6 (panels c and d); as for CaD, the P and R data points for each N value are offset from each other, for clarity.

We first address the results for CaH (B, $v' = 0$). A linear fit of $f(N) = a + bN$ to the difference data returns parameters of $a = -0.738$ ($\pm$ 0.085) cm^{-1} and $b = -0.782$ ($\pm$ 0.019) cm^{-1}, with the parameter b being associated with γ_0'. In contrast to the CaD data, one finds that $a \neq b/2$ but is offset by approximately -0.4 cm^{-1}; although this value may seem small, it is nevertheless considered to be genuine. The value is larger than any measurement uncertainty (maximal value of $\sim$0.2 cm^{-1}); moreover, approximately the same value for γ_0' is returned when the P- or R-line pairs, which originate from far separated spectral regions, are fitted independently. Furthermore, applying the conversion procedure for parameters for the two isotopomers CaH and CaD to the spin splitting parameter, utilizing $\rho = (\mu_{CaD}/\mu_{CaH})^{1/2} = 1.39664$, one calculates $\gamma_0'(CaH) = \rho^2\gamma_e'(CaD) - {}^1/_2\rho^3\alpha_\gamma'(CaD) = -0.796$ cm^{-1} from the CaD parameters that are listed in Table 2. This deviates only by $\sim$1.5% from the value returned in the CaH data fit and is well within the uncertainty of that fit ($\sim$3%).

Inspecting the data points more closely, one recognizes a small deviation from a linear relationship for the lowest two CaH (B, $v' = 0$) data points; specifically, the value for $N' = 1$ is well off the linear fit line, although its measurement error is one of the smallest. All this information is indicative that, for the lowest rotational levels ($N' < 2$), one seems to approach a level perturbation: the level splitting starts to deviate from the linear γN relation, and beyond the perturbation, an apparent level offset may be encountered.[13,22]

For the CaH(B, $v' = 1$) band system, the situation is very different. The spin splitting that is derived from the observed L_1/L_2 line pairs, which are associated with the F_1/F_2 subsystems, exhibit a complete deviation from a linear relationship, and a clear double-sequence of lines is evident (see Figure 6, trace d). No linear fit of the nature $f(N) = a + bN$ can be applied. However, inferring the spin splitting parameter for this vibrational level once again from the isotopomer values of CaD, one deduces $\gamma_1'(CaH) \cong -0.765$. Plotting the γN relation (the diamond-shaped symbols and dashed line in the lower panel of Figure 8) suggests that, indeed, the isotopomer method provides reasonable numerical values, and the expected data behavior near and beyond the perturbation level is reproduced.

Note that, in principle, it would be possible to compare the spin splitting results obtained in this work with those displayed/discussed in Figure 7 in the work of Martin;[12] because of the much higher equilibrium temperature in the reaction that yields CaH, rotational levels up to $N' \approx 30$ were evaluated, based on experimental data of that work and earlier measurements.[10] However, such a direct comparison is unfortunately not possible, because of an evident discrepancy in the energy scale of the figure. Digitizing the data and executing a linear fit results in a slope of $\sim$0.59−0.64 cm^{-1} for the spin splitting of the two vibrational states (B, $v' = 1$, 2). The derived slopes and associated γ_v' values disagree with the published value of $\gamma_e' \cong -0.8$ cm^{-1}. Unfortunately, only the R_2- and P_2-lines are listed in the publication; therefore, no re-evaluation of the data was possible.

3.3.3. Determination of the Rotational Parameters B_v and D_v. In principle, it should be possible to also derive other spectroscopic parameters from the evaluation of the line spectra and the related upper energy levels in the transitions, namely, at least the rotational constants B_v'. The "pure" rotational energy (T_{rot}) contribution associated with $B_v'N(N + 1)$ can be deter-

mined from a plot of the rotational energy level terms T_1 and T_2 versus $N(N + 1)$, by first subtracting the spin splitting component, and then providing the zero-point for T_{rot} by subtracting $T_1(N' = 0)$ from all T_1 and T_2 values.

In addition to the experimentally determined values for CaH, we also included values derived from those for CaD, based on the isotopomer conversion approach $B_v'(\mathrm{CaH}) = \rho^2 B_e'(\mathrm{CaD}) - \rho^3 \alpha_e'(\mathrm{CaD})(v + {}^1/_2)$. The agreement is good, within 1%−2%; this is consistent with the results obtained for the spin splitting parameters γ_v' and, thus, suggests that the isotopomer conversion procedure is reasonably reliable.

For increasing values of N, the distortion correction D_v normally needs to be considered, with quadratic energy contribution $D_v[N(N + 1)]^2$. The respective fits yield improved agreement between the calculated and observed T_1 term values, within the experimental uncertainty of approximately ±0.2 cm^{-1}.

The results for all derived rotational parameters B_v' and D_v' for CaH and CaD are summarized in Table 2, together with known literature values.

We would like to highlight one interesting aspect for CaH (B, $v' = 0$). When comparing the experimental data with the linear-fit and quadratic-fit reconstruction, complete agreement with the experimental values for T_1 was observed. However, for T_2, a noticeable discrepancy of the order of ∼0.4 cm^{-1} remained, which is well outside the measurement errors but is consistent with the offset of the same order of magnitude that is observed for the spin splitting data. (For relevant data, see Table S.2, provided in the Supporting Information section.)

An error in wavelength calibration can be excluded, because the transition lines for the determination of T_1 and T_2 are from the same spectral segment, which was calibrated using three Ne lines (namely, at 630.479, 633.443, and 638.299 nm) recorded in an optogalvanic resonance cell, and fringes from a Fabry−Perot Etalon. Consequently, we conclude with strong confidence, that, as suspected, the F_2 level sequence in CaH (B, $v' = 0$) is perturbed at $N' \approx 0$ or 1.

Finally, note that the reported literature values of B_v and D_v (for CaH) and those derived in this study exhibit a slight discrepancy (see Table 2). This can be attributed to the fact that much fewer and lower rotational energy levels were included in our (polynomial) fits.

3.4. Rotational Level Population in CaR ($X\,^2\Sigma^+$, $v'' = 0$). Finally, we attempted to extract information about the distribution of the rotational energy level population in the ground state of the CaH isotopomers. Because of the multicollision environment during the CaR formation, almost complete thermal equilibration of the rotational population might be expected. Indeed, all CaR spectra (see Figure 4) exhibit the common rotational line intensity pattern expected from a thermalized population of rotational levels. This is true for almost all band systems that are related to the two sublevel systems F_1 and F_2; only for the transitions into the heavily perturbed F_2-level sequence of CaH (B, $v' = 1$) is this pattern not repeated. In addition, the envelop of the intensity pattern of all rotational sequences, and the maximum observed rotational level, are approximately equal for both isotopomers. This suggests that the equilibrium temperatures T_{rot} for the (X, $v'' = 0$) ground state of CaH and CaD are different (in fact, larger for CaH).

In absorption spectra, the equilibrium the (rotational) temperature can be extracted using standard Boltzman plot procedures. However, our experimental CaR signals are related to the (1 + 1′) REMPI process: $\mathrm{CaR} - \lambda_1 \rightarrow \mathrm{CaR}^* - \lambda_2 \rightarrow \mathrm{CaR}^+$. This constitutes a two-step double-absorption scheme, and the Boltzmann plot procedure is not so straightforward. Therefore, we opted for a different approach, in which the population distribution in the ground state of CaR was derived from the experimental data by first generating synthetic spectra, taking into account the (approximate) transition probabilities for the (1 + 1′) REMPI scheme (in first approximation, the product of the electronic Einstein coefficient, the vibrational FCF value, and the rotational Hönl-London factor), and then altering the population parameter T_{rot} in a least-squares fit procedure until the best agreement with the experimental data was obtained.[23] Individually, all observed P- and R-branches of CaD, or CaH, did exhibit line intensity distributions that are consistent with a single rotational temperature, with the exception of two branch sequences that involved the perturbed F_2 levels of CaH (B, $v' = 1$). The derived average rotational temperatures were $T_{rot} = 52 \pm 7$ K for CaD (X, $v'' = 0$) and $T_{rot} = 85 \pm 11$ K for CaH (X, $v'' = 0$).

The different rotational temperatures observed for the two isotopomers might be interpreted in the following way. For the generation of CaR, the molecular reagents H_2/D_2 were added to the rare-gas carrier in a very high concentration. As noted in Section 2, the gas backing pressure was always 2.0 bar of helium and ∼0.5 bar H_2 or D_2; the gas pressure and the flow rate through the pulsed nozzle were kept constant to better than 5%. Overall, the ground-state reaction $Ca + H_2/D_2$ is endoergic: in regard to the reaction(s) that lead to the product CaR (X) in the exit channel, CaH (X) is less endoergic than CaD (X), by ∼450 cm^{-1}. The laser sputtering process provides sufficient energy (either internal or kinetic energy), so that the product CaR (X) is formed with reasonable efficiency. After the formation of CaR (X), the level population thermalizes, via collisions with He/H_2 (D_2) in the continuing beam expansion. Both energy-level structures in CaD and D_2 are denser than for their hydrogen equivalents; this means that thermal equilibration in collisions should be more favorable, yielding lower temperatures for CaD.

As a final remark, we would like to note that the observed line intensities exhibited slightly irregular amplitude patterns that were not consistent with the absorption spectra from a thermalized ground-state population. These irregularities were observed for both CaH and CaD. Although, for the former, one could possibly argue that the $A\,^2\Pi/B\,^2\Sigma^+$ level perturbation might be responsible, CaD does not exhibit any such interaction. One therefore might speculate about some reaction-dynamics "history"; however, we think it to be unlikely that any would still be observable under the experimental conditions for CaR formation and evolution. The residence time inside the reaction canal of a few tens of microseconds, and the multiple-collision environment strongly favor thermalization of the rotational level population. Also, contributions from any other precursor source (e.g., the photolysis of calcium hydroxide ($Ca(OH)_2$)) are very unlikely. Although occasionally the calcium hydroxyl fragment (CaOH) was observed early in experimental runs (thought to be related to surface contamination of the Ca disk), the homologous fragment CaOD was never observed.

A likely explanation may be found in the ionization step of the excitation sequence. The ionization is not into a "smooth" continuum (which, generally, is a reasonable assumption for the majority of polyatomic molecules) but rather into a molecular ion state that exhibits a similar energy level structure as the neutral precursor molecule. Thus, with respect to our CaR experiments, when the ionizing radiation λ_2 is changed from its fixed-wavelength value of 266.2 nm to a tuneable laser wavelength, it should be feasible to probe the unknown rotational level structure in CaH^+ (X; v^+, N^+). Preliminary

theoretical calculations that we performed, which were based on the ab initio data for CaH^+,[24] suggest that such a structure should be resolvable, and the preparation of related experiments is underway.

4. Conclusion

We have demonstrated a sensitive approach of generating and probing metal hydride radicals, which normally are not easily investigated in the gas phase; the principle was exemplified for CaR (R = H, D). These isotopomers were prepared in their electronic ground-state ($X\ ^2\Sigma^+$) in a laser-evaporated atomic pulsed gas chemical reaction, yielding a population in low quantum numbers via supersonic expansion cooling after generation of the radical.

The sensitive, high-resolution detection of transitions with a low rotational quantum number, in the range of $N = 0, ..., 10$, allowed us to extract spectroscopic parameters for the intermediate state CaR ($B\ ^2\Sigma^+$, $v' = 0, 1$). Specifically, we determined values for the spin-splitting parameter $\gamma_{v'}$. In the case of CaD, these had not been measured previously; in the case of CaH, the previous estimate[11] has been confirmed, and, in addition, the change of $\gamma_{v'}$ with the vibrational quantum number N was quantified. The estimates for the rotational and distortion parameters, $B_{v'}$ and $D_{v'}$, are consistent with some of the published CaH data.[12,25] Once again, in the case of CaD, these parameters were determined for the first time.

The observed spectra also confirm the perturbation of all vibrational levels CaH ($B\ ^2\Sigma^+$; v'), for low rotational quantum states in the F_2 subsystem, by the ($A\ ^2\Pi$; $v' + 1$) states. Specifically, the onset of perturbation in the vibrational level $v' = 0$, near $N' = 0/1$, was proven; this had not been recognized previously (in the studies of Berg and co-workers in the 1970s and 1980s, transitions with high N values dominated the spectra). This perturbation should be completely absent in CaD, because of the substantially different level spacing of the isotopomer; indeed, this was confirmed in our study, and we demonstrated how the spectroscopic parameters of the unperturbed species could be used to analyze (de-perturb) the perturbed levels of the other isotopomer.

When extracting the population distribution in the rotational levels of the ground state ($X\ ^2\Sigma^+$; $v'' = 0$) from the spectral line intensities, it was noticed that, although a Boltzmann distribution is generally observed, slight scatter of the data points was encountered in all recorded rovibrational band systems, both for CaD and CaH. It can be argued that, most likely, the rotational energy level structure in the final ion state CaR^+ ($X\ ^2\Sigma^+$; v^+; N^+) is responsible for this behavior, and that the ionization step in the ($1 + 1'$) REMPI scheme may not be constant, as is normally assumed. The concept that rotational and vibrational levels in the ion CaR^+ can, indeed, be probed in this way will be subject of a series of experiments that are currently underway, in which the laser radiation for ionization will be tunable rather than fixed, as was the case in this study.

The apparent rotational temperatures (T_{rot}) were different for CaH and CaD, although all experimental parameters were kept constant as much as possible. This phenomenon is thought to be due to a more efficient cooling of CaD, with a denser energy level structure, in an environment with a molecule of equally denser level structure, namely D_2 (the amount of the hydrogen reactant was substantially higher—4:1 ratio for the $He:H_2$ (D_2) gas mixtures—than is normally the case for supersonic expansion cooling in a rare-gas carrier). We think that this might be exploitable in experiments for the Zeeman trapping of (rotationally cold) molecules, which has been demonstrated for CaH (X; $v'' = 0$; $N'' = 0$; $J'' = {}^1/_2$).[26,27] In principle, CaD could be prepared with a rather narrow, cold rotational population distribution (with an overall lower internal energy than CaH), and subsequently this distribution might be depleted selectively by ($1 + 1'$) REMPI. The ultimate goal would be the generation of single-rotational-state precursor molecules, which will, ultimately, be trapped. Experiments are currently in preparation to explore the feasibility of such a selective depletion of individual rotational energy levels.

Acknowledgment. Financial support for this work from MCyT Grant No. BQU2001-1461 and from the Ramón Areces Foundation is gratefully acknowledged. H.H.T. thanks the Spanish Ministerio de Educación, Cultura y Deporte for a Sabbatical Research Fellowship.

Supporting Information Available: A complete list of line positions and rotational energy levels used in the data evaluation, as well as a comparison between measured and calculated term values using the parameters in Table 2. This material is available free of charge via the Internet at http://pubs.acs.org.

References and Notes

(1) Barbuy, B.; Schiavon, R. P.; Gregorio-Hetem, J.; Singh, P. D.; Batalha, C. *Astronom. Astrophys. Suppl. Ser.* **1993**, *101*, 409.
(2) Balfour, W. J.; Klynning, L. *Astrophys. J.* **1994**, *424*, 1049.
(3) Simard, B.; Mitchell, S. A.; Humphries, M. R.; Hackett, P. A. *J. Mol. Spectrosc.* **1988**, *129*, 186.
(4) Shirley, J. E.; Scurlock, C. T.; Steimle, T. C.; Simard, B. *J. Chem. Phys.* **1990**, *93*, 8580.
(5) Balfour, W. J.; Cao, J.; Qian, C. X. W.; Rixon, S. J. *J. Mol. Spectrosc.* **1997**, *183*, 113.
(6) Skowronek, S.; Pereira, R.; González Ureña, A. *J. Phys. Chem. A* **1997**, *101*, 7468.
(7) Brugh, D. J.; Morse, M. D. *J. Chem. Phys.* **1997**, *107*, 9772.
(8) Simard, B.; Hackett, P. A.; Balfour, W. J. *Chem. Phys. Lett.* **1994**, *230*, 103.
(9) Barnes, M.; Merer, A. J.; Metha, G. F. *J. Mol. Spectrosc.* **1995**, *173*, 100.
(10) Pereira, R.; Skowronek, S.; González Ureña, A.; Pardo, A.; Poyato, J. M. L.; Pardo, A. H. *J. Mol. Spectrosc.* **2002**, *212*, 17.
(11) Berg, L. E.; Klynning, L.; Martin, H. *Opt. Commun.* **1976**, *17*, 320.
(12) Martin, H. *J. Mol. Spectrosc.* **1984**, *108*, 66.
(13) Herzberg, G. *Molecular Spectra and Molecular Structure: I. Spectra of Diatomic Molecules*, 2nd ed.; Van Nostrand: New York, 1950.
(14) Watson, J. K. G. *J. Mol. Spectrosc.* **1980**, *80*, 411.
(15) Hulthèn, E. *Phys. Rev.* **1927**, *29*, 97.
(16) Berg, L. E.; Klynning, L. *Astron. Astrophys. Suppl. Ser.* **1974**, *13*, 325.
(17) Berg, L. E., private communication, 2001.
(18) Petitprez, D.; Lemoine, B.; Demuynck, C.; Destombes, J. L.; Macke, B. *J. Chem. Phys.* **1989**, *91*, 4462.
(19) Telle, H. H.; Telle, U. *Comput. Phys. Commun.* **1982**, *28*, 1.
(20) Leininger, T.; Jeung, G. *J. Chem. Phys.* **1995**, *103*, 3942.
(21) Frum, C. I.; Pickett, H. M. *J. Mol. Spectrosc.* **1993**, *159*, 329.
(22) Kovacs, I. *Rotational Structure in the Spectra of Diatomic Molecules*; Adam Hilger: London, U.K., 1969.
(23) Al-Tuwirqi, R. M. A. *Simulation of Absorption and Emission Spectra of Diatomic Molecules Generated in Molecular Beams*, Ph.D. Thesis, University of Wales Swansea, Swansea, U.K., 2000.
(24) Boutalib, A.; Daudy, J. P.; El Mouhtadi, M. *Chem. Phys.* **1992**, *167*, 111.
(25) Martin, H. *J. Chem. Phys.* **1988**, *88*, 1797.
(26) Weinstein, J. D.; deCarvalho, R.; Guillet, T.; Friedrich, B.; Doyle, J. M. *Nature* **1998**, *395*, 148.
(27) Friedrich, B.; Weinstein, J. D.; deCarvalho, R.; Doyle, J. M. *J. Chem. Phys.* **1999**, *110*, 2376.